https://doi.org/10.5194/egusphere-2023-2056
Preprint. Discussion started: 6 October 2023

Summertime tropospheric ozone source apportionment study in Madrid (Spain)

David de la Paz[1], Rafael Borge[1], Juan Manuel de Andrés[1], Luis Tovar[1], Golam Sarwar[2], Sergey L. Napelenok[2]

[1]Laboratory of Environmental Modelling, Department of Chemical & Environmental Engineering, Universidad Politécnica de Madrid, (UPM), c/ José Gutiérrez Abascal 2, 28006, Madrid, Spain

[2]Center for Environmental Measurement & Modeling, U.S. Environmental Protection Agency, Research Triangle Park, NC, USA

Correspondence to: Rafael Borge (rafael.borge@upm.es)

Abstract. The design of emission abatement measures to effectivly reduce high ground-level ozone (O_3) concentrations in urban areas is very complex. In addition to the strongly non-linear chemistry of this secondary pollutant, precursors can be released by a variety of sources in different regions and locally produced O_3 is mixed with that transported from the regional or continental scales. All of these processes depend also on the specific meteorological conditons and topography of the study area. Consequently, high-resolution comprehensive modeling tools are needed to understand the drivers of photochemical pollution and to assess the potential of local strategies to reduce adverse impacts from high tropospheric O_3 levels. In this study, we apply the Integrated Source Apportionment Method (ISAM) implemented in the Community Multiscale Air Quality (CMAQv5.3.2) model to investigate the origin of summertime O_3 in the Madrid region (Spain). Consistent with previous studies, our results confirm that O_3 levels are dominated by non-local contributions, representing around 70% of mean values across the region. Nonetheless, precursors emitted by local sources, mainly road traffic, play a more important role during O_3 peaks, with contributions as high as 25 ppb. The potential impact of local measures is higher under unfavorable meteorological conditions associated with regional accumulation patterns. These findings suggest that this modeling system may be used in the future to simulate the potential outcomes of specific emission abatement measures to prevent high-O_3 episodes in the Madrid metropolitan area.

1. Introduction

Air pollution is one of the main environmental problems and is recognized as a global threat to public health. In 2019, 4.2 million people died prematurely worldwide as a result of a poor air quality (WHO, 2021). Even in regions that have taken decisive actions to curb emissions, such as Europe, over 300,000 premature deaths (EU27) are currently associated to air pollution, most of them related to high levels of $PM_{2.5}$ (particles with aerodynamic diameter of ≤ 2.5 microns) (238,000) and NO_2 (nitrogen dioxide) (49,000) (EEA, 2022). In recent years, concentrations of many of the regulated pollutants in Europe have decreased as a result of a general reduction of emissions. From 2009 to 2018, the concentration of PM_{10} (particles with aerodynamic diameter of ≤ 10 microns), $PM_{2.5}$ and NO_2 diminished on average by 19%, 22% and 18-23% (depending on the air quality monitoring station type), respectively (EEA, 2020). These measures, however, have failed to significantly improve ozone (O_3) ambient concentration levels.

Tropospheric O_3 is a secondary pollutant formed from photochemical reactions between many different precursors, mainly nitrogen oxides (NO_x = NO (nitric oxide) + NO_2) and non-methane volatile organic compounds (VOCs) (Seinfeld and Pandis, 2016; Jenkin and Clemitshaw, 2000; Monks et al., 2015). According to the last European Union (EU) emission inventory report (EEA, 2022), the most important activity sectors regarding O_3 precursors emissions are the "Road transport" sector (7% and 37% of total VOCs and NO_X emissions, respectively), the "Commercial, institutional and households" sector (15% and 14%, respectively) and the "Solvent and product use" sector, representing 42% of total VOCs emissions. Once emitted from urban and industrial areas, these precursors are subsequently transported by the prevailing wind regime (Xu et al., 2011).

https://doi.org/10.5194/egusphere-2023-2056
Preprint. Discussion started: 6 October 2023

Atmospheric life-time of O_3 depends on numerous variables. In the boundary layer, atmospheric life-time of O_3 is short, roughly 1 or 2 days, depending on the abundance of precursors (Young et al., 2013). In the free troposphere, its lifetime can be of up to 2 weeks, time enough to be transported long distances, from the local to the global scale (Monks et al., 2015; Stevenson et al., 2006). In addition to in-situ formation, transport of O_3 from the stratosphere is also relevant to explain the tropospheric ozone concentration (Ipcc, 2007; Hsu et al., 2005). Furthermore, this gas exchange between layers of the atmosphere is expected to increase in the future (Meul et al., 2018; Banerjee et al., 2016).

Due to these complex dynamics, tropospheric O_3 levels have not decreased (Jung et al., 2022; Sicard et al., 2023) in accordance to significant NO_X and VOCs emissions reduction (45% and 41%, respectively in the 2009- 2018 period). As a result, 12% of the urban population in Europe is still exposed to high O_3 concentrations according to EU regulations, with a toll of 24,000 premature annual deaths (EEA, 2022), especially in the Mediterranean basin (Amann, 2008; EEA, 2018, EEA2020). The share of urban population that suffers from excessive exposure to O_3 rises to 95% (EEA, 2022) when the World Health Organization (WHO) guidelines are considered (WHO, 2021). Of note, tropospheric O_3 produces both short-term (Bates et al., 1972; Bell et al., 2004; Goodman et al., 2018) and long-term health effects (Jerrett et al., 2009; Seltzer et al., 2018), impacting the population living in large urban agglomerations as well as their surroundings. Moreover, it also may have relevant effects on ecosystems (De Andrés et al., 2012; Mills et al., 2011; Harmens et al., 2011) and climate (Sitch et al., 2007; Stocker et al., 2013; IPCC, 2015).

Globally, the latest studies using satellite data suggest that tropospheric O_3 average concentration levels increased over the last four decades (Ziemke et al., 2019; Gaudel et al., 2018). (Paoletti et al., 2014) evaluated observations from monitoring stations in the United States (US) and Europe from 1990 to 2010 and concluded that the O_3 annual average increased by 7%/year in rural stations and around 12-17%/year (US and EU, respectively) in urban stations. However, O_3 formation is highly non-linear and trends may change depending on the evaluated time period and region, the metric used, and other local factors such as topography or the proximity to the precursor's emission sources (Reche et al., 2018; Massagué et al., 2023). According to specific studies for the Iberian Peninsula, the trend of the annual average of O_3 for rural stations in the 2004-2012 period was not clear (Querol et al., 2014). In contrast, an increasing trend around 1 – 3%/year was observed in all seasons in urban, traffic and industrial stations. (Borge et al., 2019) reported an average increase of 10 $\mu g \cdot m^{-3}$ of daily 8-hour maximum O_3 moving average concentrations (MDA8) for the 1993-2017 period. However, they detected that the highest increase related to fall and winter months (up to 19 $\mu g \cdot m^{-3}$), in agreement with general increases of the oxidation capacity in the atmosphere of the largest urban areas in Europe modeled by Jung et al. (2022).

Nonetheless, the O_3-forming photochemical activity is largely regulated by weather conditions, especially temperature and solar radiation. For this reason, tropospheric O_3 formation has a marked seasonal character, with the highest O_3 concentration values typically recorded in spring and summer (Logan, 1985; Granados-Muñoz and Leblanc, 2016), especially in those locations that are highly influenced by nearby urban areas (Brodin et al., 2010; Carnero et al., 2010) where large amounts of precursors are emitted. Therefore, understanding summertime O_3 dynamics is more relevant from air quality management perspective.

This research focuses on the center of the Iberian Peninsula, encompassing the city of Madrid and its surroundings. Consistently with general emission trends in Europe, the emission of the main O_3 precursors in the Madrid Region decreased by 47%, for VOCs, and by 44% for NO_X from 1990 to 2018 (CM, 2021). While recent control measures succeeded in reducing NO_2 levels (AM, 2022), such emissions reductions have, at the same time, substantially impacted urban atmospheric chemistry by modifying its oxidative capacity. Recent studies (Saiz-Lopez et al., 2017; Querol et al., 2016) suggest that O_3 concentration levels have increased in Madrid by 30-40% during the 2007-2014. A greater decrease in NO emissions than in NO_2 emissions (with the subsequent reduction of the NO/NO_2 ratio) may be one of the factors responsible for this response (Querol et al.,

https://doi.org/10.5194/egusphere-2023-2056
Preprint. Discussion started: 6 October 2023

2016; Querol et al., 2017; Zaveri et al., 2003; Jhun et al., 2015). The exceedances of the target value for the protection of human health mainly occur in summer periods, especially under adverse meteorological conditions that have been extensively characterized in previous studies (Querol et al., 2016; Querol et al., 2017; Millan et al., 2000; Plaza et al., 1997; Querol et al., 2018; Pay et al., 2019; Escudero et al., 2019).

In this research, we apply a state-of-the-science air quality model to provide insights into the emission sources and transport patterns which are involved in the formation of tropospheric O_3 during typical summertime conditions in the Madrid region. In addition to contributing to the scientific understanding of photochemical pollution, the final purpose of this work is to inform the decision-making process needed to design further emission reduction measures in the study area.

2. Methodology

2.1. Modeling system

The research is supported by a mesoscale modeling system with three main components. Meteorological fields are generated by WRFv3.7.1 (Weather Research and Forecasting) (Skamarock and Klemp, 2008). Physics options and parameterizations (Table S1 in the supplement) are based on previous studies (Borge et al., 2008a; de la Paz et al., 2016) and WRF outputs were postprocessed with MCIP v5.1 (Meteorology - Chemistry Interface Processor) (Otte and Pleim, 2010). Emission processing relies on the US EPA SMOKEv3.6.5 (Sparse Matrix Operator Kernel System) model (Institute and Environment, 2015; Baek and Seppanen, 2018) that has been specifically adapted for the Iberian Peninsula (Borge et al., 2008; Borge et al., 2014). Biogenic emissions are generated by MEGAN v2.1 (Model Emissions Gases and Aerosols from Nature) (Guenther, 2006; Guenther et al., 2012). The third component is the CMAQv5.3.2 (Community Multiscale Air Quality) modeling system (Byun and Schere, 2006; Ching and Byun, 1999). This 3D chemical-transport model (CTM) simultaneously predicts the concentration of all relevant substances considering transport (advection and diffusion), chemical transformation and deposition. Gas-phase atmospheric chemistry is represented by the Carbon Bond 6 (CB06) (Yarwood et al., 2010) chemical mechanism with chlorine chemistry (CB06r3) (Sarwar et al., 2012; Whitten et al., 2010, Emery et al., 2015) according to SPECIATE 4.0 (Hsu et al., 2006) while the module AERO6 (Appel et al., 2013) is used to describe aerosol dynamics and chemistry. Considering the influence of different scales, from the continental to the regional-urban, on O_3 levels (Valverde et al., 2016; Pay et al., 2019; Baker et al., 2016; Han et al., 2018), boundary conditions are of particular interest. Previous studies in the Iberian Peninsula have demonstrated that O_3 is particularly sensitive to boundary conditions (Borge et al., 2010). For a more realistic representation of the boundary influence, the mother domain receives dynamic chemical boundary conditions from hemispheric CMAQ (Mathur et al., 2017) simulations.

Source attribution provides information on the relative importance of emissions sources on ambient concentration levels which can be particularly useful for highly non-linear secondary pollutants such as O_3 (Cohan and Napelenok, 2011). In this study, the Integrated Source Apportionment Method (ISAM) (Kwok et al., 2015; Kwok et al., 2013) implemented in CMAQv5.3.2 (Napelenok, 2020b) is used. This mass-transfer method tracks the contribution of all the precursors and proportionally attributes the products to the corresponding sources (Napelenok, 2020a). While this approach is based on the same conceptual basis, it substantially differs from the implementation of previous versions (including CMAQv5.0.2) that attribute the formation of a secondary pollutant to the sector contributing the limiting reactant. While other source apportionment approaches (Thunis et al., 2019) based on sensitivities may be better suited to investigate the potential of abatement measures (Borge et al., 2014), tagging methods such as ISAM can serve better for diagnosis purposes (Borge, 2022) and thus, can be successfully applied to study pollution dynamics (Simon et al., 2018; Li et al., 2022; Pay et al., 2019).

https://doi.org/10.5194/egusphere-2023-2056
Preprint. Discussion started: 6 October 2023

2.2. Modeling domains

The three nested domains shown in Figure 1 were used to perform the numerical simulations in this study. This layout is intended to capture medium (Millán et al., 1991) and long-range influences of O_3 transport (Zhang et al., 2020; Qu et al., 2021; Brook et al., 2013) and to provide enough resolution over the area of interest to depict local dynamics (Plaza et al., 1997; Borge et al., 2022). The mother domain (D1) includes Europe and Northern Africa with a 12 km x 12 km spatial resolution while D2 is centered over the Iberian Peninsula and has a 4 km x 4 km spatial resolution (Table S2 in supplement). The innermost domain (D3) used in this study covers Madrid and surroundings with 1 km^2 spatial resolution (136 km in the east-west direction and 144 km in the north-south direction). All three domains have a common 35-level vertical structure covering the whole Troposphere with 18 layers within the first kilometer to accurately represent atmospheric processes within the planetary boundary layer (Borge et al., 2010).

The region has a continental Mediterranean climate with an annual mean temperature of 14.6 ºC and 367 mm of accumulated precipitation with a typical summer drought (https://www.madrid.org/iestadis/fijas/coyuntu/otros/cltempe.htm). The Central Range (Sierra de Guadarrama), with maximum elevations of 2500 meters above sea level (m.a.s.l.), crosses the D3 modeling domain in the NE-SW direction and divides it into two main regions; the northern and southern plateaus of the Iberian Peninsula. The southern half of the domain, where the city of Madrid (with an average elevation of 657 m) is located, features the Tajo river basin. This topography configures a dominant wind circulation along the NE-SW direction and enhances anticyclonic stagnation conditions (Plaza et al., 1997; Querol et al., 2018) usually induced by the semi-permanent Azores High (García et al., 2002). O_3 formation typically peaks with high temperature and solar radiation under stagnation conditions (Querol et al., 2018; Reche et al., 2018; Garrido-Pérez et al., 2020) that often occur at summertime.

2.3. Temporal domain

Model simulations were completed for July 2016, using a previous 3-day period as model spin-up. According to the Spanish Meteorological Agency (AEMET, 2017) it was an unusually warm month (with an average temperature of 25.5 ºC), being the 4th hottest month of July since 1961 in the Iberian Peninsula. It was also a dry month, with 13% less precipitation than the average of the month in the 1981-2010 reference period. Considering the meteorological trends in this region (Borge et al., 2019), it may be considered as a representative summer period for modern weather conditions. More importantly, this period was selected because of an intensive experimental campaign carried out to characterize ozone episodes in Madrid and surroundings (Reche et al., 2018). This period was thoroughly analyzed by (Querol et al., 2018) that identified two typical circulation patterns associated to venting and accumulation episodes. The later are characterized by weak wind forcing (wind speed <4-5 m s^{-1}), stable conditions and air stagnation that favor O_3 local formation. Oppositely, stronger winds (> 7 m s^{-1}) promote advection and prevents from reaching O_3 peaks under venting conditions.

During this period (2016), 26 out of the 42 air quality monitoring stations in the innermost (D3) modeling domain (Figure 1), recorded exceedances of the concentration threshold related to the O_3 target value for the protection of human health (MDA8 > 120 $\mu g \cdot m^{-3}$). The highest number of exceedances (up to 359 in the month, 47% of total annual exceedances) were found around the Madrid metropolitan area, in the city outskirts. Of note, no exceedances of the MDA8 were recorded downtown Madrid.

2.4. Emission sources for the apportionment analysis

Emissions for this modeling exercise result from the combination of the official national (MMA, 2018), regional (CM, 2021) and Madrid's city local inventory (AM, 2022), conveniently adapted and spatio-termporally resolved for modeling purposes (Borge et al., 2018). Total annual NO_X and VOCs emissions aggregated by SNAP (Selected Nomenclature for Air Pollution) groups are summarized in Figure 2. Emissions from power generation and industrial activities (SNAP 01, SNAP 03 and SNAP

https://doi.org/10.5194/egusphere-2023-2056
Preprint. Discussion started: 6 October 2023

034) were merged due to their limited presence in this modeling domain. Since emissions from agriculture (SNAP 10) in the region are only significant for VOCs from plants, they have been tagged along biogenic VOC emissions from vegetation (SNAP 11). Consequently, 8 major sources were tagged for the source apportionment analysis of ambient O_3 in the region. They account for the totality of emissions in the modeling domain although the main precursors originate from road traffic (SNAP 07) and solvent use (SNAP 06), with a total share of 65% NO_X and 49% VOCs, respectively. While emissions from the residential, commercial and institutional sector (SNAP 02) account for nearly 19% of annual NO_X emissions, they are produced almost exclusively in winter and are therefore, negligible in summer.

In addition to the attribution of O_3 concentration to the emissions within the modeling domain, hereinafter referred to as local sources, the contribution of boundary conditions (BC) and initial conditions (IC) are also estimated in this study. Considering the typical O_3 daily patterns and the variability of circulation patterns, the latter refer to the initial concentration on a daily (24 hour) basis, i.e., each day is run separately using the concentrations from the previous day as IC.

3. Results

The results are presented in three subsections. Firstly, an overview of the source apportionment analysis carried out in the study area for the whole month is discussed. Then, this same analysis is performed for two specific days representative of different circulation patterns defined by (Querol et al., 2018): advective pattern (July 13th) and accumulation pattern (July 27th). Additional information for July 20th and July 6th, identified by Querol et al. (2018) as advective and accumulation days, respectively, is provided in the supplement. Finally, the temporal patterns of the O_3 apportionment are examined at the location of the air quality monitoring stations within in the simulation domain. Aggregated results by station type are discussed in 3.3 while the results for different geographical areas relative to the location of Madrid city (quadrants) are presented in the supplement.

3.1. Spatial analysis of the source apportionment assessment

Figure 3 shows the contribution to ground-level O_3 concentration of the BC and that of all local anthropogenic emissions combined. O_3 apportionment to biogenic emissions is not considered in Figure 3 because i) they have less interest from the point of view of possible abatement measures (Oliveira et al., 2023) and ii) their contribution is relatively small (below 3%.) This is in contrast with apportionment studies done at global or continental scales elsewhere (Butler et al., 2020; Li et al., 2023), but is consistent with recent studies based on a more comparable methodology for the Iberian Peninsula specifically (Pay et al., 2019).

Both monthly average and high concentration values (illustrated by the 90th percentile, hereinafter P90) come mostly from BC. This is consistent with previous studies that have identified boundary conditions as the dominant contribution to ground-level O_3, i.a. Pay et al. (2019) for the Iberian Peninsula, (Collet et al., 2018) for the USA or (de la Paz et al., 2020) for Madrid. However, the weight of each of the sources on both metrics is different. As an average, 70% of the mean O_3 concentration in the Madrid region comes from BC (Figure 3a), while for P90, the contribution from BC is considerably smaller, around 50% (Figure 3b). The maximum anthropogenic contribution for the monthly average (Figure 3c) reaches 17% (7.5 ppb in absolute terms), with a mean contribution of 8% over the whole Madrid Region (Figure S1). Regarding P90 (Figure 3d), the maximum contribution is 28% (in the center and southwest of the Madrid municipality), around 22 ppb in absolute terms, and a slightly higher mean contribution over the Madrid region as a whole (14%, 11 ppb as shown in Figure S1). Despite the general dominance of BC on O_3 concentration, these results point out the relevance of local emissions (Figure 2) is higher for O_3 peaks.

Figure 4 shows the apportionment of each emission sector for local sources. Road transport (SNAP07) is the most influential sector, with an average contribution in the Madrid region of 41% and with maximum contributions of around 55%, located in

https://doi.org/10.5194/egusphere-2023-2056
Preprint. Discussion started: 6 October 2023

the proximity of the main communication routes (Figure 4d). In absolute terms, this means an average contribution of 5 ppb and a maximum one of 11 ppb (Figure S2). The next sector with the highest contribution relates to off-road mobile sources (SNAP08), with an average contribution in the Madrid region of 17% (1.8 ppb) and a maximum of 8 ppb in the vicinity of the Adolfo Suárez Madrid-Barajas airport.

The contribution of the use of solvent and other products (SNAP06), the largest anthropogenic emitter of VOCs, is as low as 1.5 ppb on average in Madrid region, with maximums of 3 ppb, similar to the contribution of all industrial sources combined (SNAP01-03-04) The rest of the sectors analyzed (SNAP05 and SNAP09) have negligible contributions (around 0.05 ppb as an average over the Madrid region).

If the analysis is done on a daily basis, it is worth noting the significance of the initial conditions (IC) as well, with a spatially-averaged contribution of 19% and of 34% to monthly average and P90 concentrations, respectively (Figure S1). However, the role of IC is more relevant to analyze how meteorological conditions may affect the source apportionment. Of note, in this study IC refers to O_3 from the previous 24-hour period. Consequently, the effect of IC on O_3 does not necessarily diminish throughout the month. Instead, we found that the influence of IC relates mainly to regional circulation patterns. We elaborate on this in the following sections.

3.2. Source apportionment assessment under characteristic circulation patterns

The study of the influence of meteorology on the O_3 ambient concentration is carried out by analyzing the results for specific days representative of the two circulation patterns. Querol et al., (2018) identified an advective pattern for 13th and 20th July and an accumulation pattern for 6th and 27th July. In this section, we examine the source apportionment for those dates (13th and 27th in more detail) to test the hypothesis that local atmospheric conditions may induce a significant difference on O_3 attributions.

Figure 5 shows the daily average and the P90 of hourly O_3 concentrations during the accumulation and advective episodes. It is observed that during accumulation days (6th and 27th), the average concentration in the Madrid region was between 13 - 20% higher than that during the advective periods (days 13th and 20th), and around 4 - 8% higher than the monthly average. Regarding the maxima, the average P90 (3rd highest hourly concentration for a given day) during the accumulation periods in the Madrid region may be 25% higher than that of the ventilation periods.

3.2.1. Accumulation pattern

Consistent with previous studies that highlight the role of meteorology on O_3 (Nguyen et al., 2022), modeling results show that accumulation days are especially relevant regarding the potential impacts on health and vegetation and a deeper analysis of pollution dynamics under those conditions is of interest. Figure 6 shows the hourly evolution (3:00, 9:00; 15:00, 21:00 UTC) of surface O_3 concentrations during the day 27th (day 6th Figure S4), along with O_3, NOx and VOCs vertical concentration up to 5 km height for a NE-SW cross section, related to the dominant wind directions (the same results for a perpendicular SE-NW cross section are shown in Figure S5 in the supplement).

A low O_3 concentration surface layer (around 40 ppb) can be clearly seen for early hours of the day (03:00 UTC, 05:00 local time). This relates to a shallow Planetary Boundary Layer (PBL) (a few hundred meters high) and weak winds from the NE (between 1-2 m s^{-1}). Around 6:00 UTC (08:00 local time), the main emitting sectors (such as road transport) begin to emit O_3 precursors (see (Quaassdorff et al., 2016) for characteristic emission temporal profiles). The prevailing surface wind directs the urban plume towards the SW and the southern slope of the Sierra de Guadarrama (Figure S3). Of note, the wind direction aloft is the opposite, in accordance with recirculation processes reported for this domain (Plaza et al., 1997). As the day progresses (09:00 UTC, 11:00 local time), the PBL height grows (up to 1.5 km) as radiation and temperature increase, mixing

https://doi.org/10.5194/egusphere-2023-2056
Preprint. Discussion started: 6 October 2023

O_3 vertically. At the same time, the emissions of precursors (concentrated in the Madrid city, MD) lead to an increase in the local production of O_3 in the plume, more evidently in the rural areas (NOx limited regions) in the leeward side of the city. On the contrary, in the vicinity of high NO_X emission intensity areas, O_3 is consumed by NO through the reaction $NO+O_3 \rightarrow NO_2 + O_2$, a titration effect documented in previous studies (Saiz-Lopez et at., 2017).

Over the following mid-day hours (09:00-15:00 UTC, 11:00-17:00 local time) the PBL further develops and a vertical homogenization process occurs. There is a deep vertical mixing of newly formed ozone with O_3-enriched upper layers generated in previous days (Querol et al., 2018; Escudero et al., 2019). As illustrated in Figure 7, there is a first O_3 reservoir located around 1500 m altitude (at 00:00 UTC, 02:00 local time) that relates mainly to local sources and contributes with 2-8 ppb, while higher O_3 reservoirs (around 4000 meters a.s.l) relate to BC and have a considerably higher contribution (50-75 ppb). Around 15:00 UTC (17:00 local time) the PBL reaches 3000 - 4000 m in accumulation periods and O_3 concentration levels up to 75 - 80 ppb are found (Figure 6). This dynamics is compatible with the ozone sounding (http://www.woudc.org/data/metadata/query_results_platform_e.html?Platform=308) included in Figure 8, that shows a very constant O_3 concentration around 65 to 70 ppb from the surface to 4000 m.a.s.l.

Later, around 17:00 UTC, the local O_3 production from anthropogenic local emissions released earlier is maximum (Figure 7), with ground-level contributions that can reach 30 ppb SE in the municipality of Madrid. However, the greatest contribution during these hours continues to be from the BC (up to 50 - 60 ppb at surface level). From 21:00 UTC, the PBL has already decreased to a few hundred meters, the turbulence dwindles, the surface flow towards the SW is re-established and the formation of enriched levels of precursors (Figure 6) and ozone (Figure 7) in the 1000-2000 meters a.s.l. occurs again, in accordance with the regional recirculation processes reported in the literature for this area (Querol et al., 2018; Escudero et al., 2019).

3.2.2. Advective pattern

As an example of an advective pattern, Figure 9 shows the plan view and the NE-SW cross section of O_3, NOx and VOCs concentration during July 13th (Figure S6 shows the SE-NW cross section for day 13th and Figure S7 and Figure S8 represent the NE-SW cross section and the SE-NW cross section for day 20th, respectively in the Supplement). It can be seen that surface O_3 concentration levels at 3:00 UTC are around 8% lower than those of July 27th (accumulation), (average in the Madrid region of 39 ppb and 42 ppb, respectively) with maximum concentrations along Sierra de Guadarrama, where elevated terrain reaches layers rich in O_3 and precursors from the lower troposphere and from the residual layers formed the day before (Figure S6). This occurs (also under accumulation conditions) when the PBL height is located below the maximum height of the Sierra de Guadarrama. However, during advective periods, a stronger stratification of the O_3 concentration is observed during the early hours (3:00 – 9:00 UTC) due to the existence of more intense wind direction speed vertical gradients (relative to accumulation conditions), perfectly captured by the modelling system (Figure 8).

At 09:00 UTC, the local O_3 production downwind of the city is lower than during the accumulation periods (Figure S9), not only quantitatively but also in terms of the total area affected. This can be explained by the weather conditions (promoting dispersion) and the corresponding lower concentration of the main precursors (5-8 ppb NOx and 15-20 ppb of VOCs on the day 13th, compared to 10-15 ppb NOx and 30-40 ppb of VOCs during accumulation day 27th). At 15:00 UTC, the PBL height increases reaching 2,500-2,800 m altitude (compared to 4,000 m on day 27th). As the PBL grows, the vertical mixing dominates the wind-driven pollution displacement in the SW direction. Similarly to the dynamics described for accumulation conditions, this allows precursors and fresh O_3 to ascend and mix existing ozone in higher layers (Figure 9 and Figure 10). Nonetheless, the vertical mixing is lower, as observed in the ozone soundings (Figure 8), with the consequent difficulty of the boundary layer to incorporate O_3 from higher strata (beyond 4000 meters a.s.l.) in the central hours of the day. This results in lower O_3 concentration at surface level under advective conditions, up to 60 ppb SW of Madrid City (Figure 9). As for the relative

https://doi.org/10.5194/egusphere-2023-2056
Preprint. Discussion started: 6 October 2023

importance of local sources, Figure 10 shows that their contribution can reach nearly 30 ppb, similar to that under accumulation conditions. However, the area affected is clearly associated with the city plume and their contribution averaged over the region is smaller. In fact, our results point out that precursors advected can produce hourly peaks above 30 ppb outside the Madrid region.

3.3. Source apportionment assessment at the location of monitoring stations

A source apportionment assessment has also been carried out at the location of the air quality monitoring stations distributed throughout the simulation domain (Figure 1) to inform on the contributions of different sources in those points where air quality is routinely monitored. Differences are found depending on the type of station (urban, suburban and rural) and, consistently with the results discussed in the previous subsection, the type of circulation pattern (advective or accumulation). The results are summarized in Figure 11.

Urban and suburban monitoring stations have a similar aggregated behavior. During the first hours of the morning, the initial and boundary conditions make up the totality of O_3 concentration until 06:00 UTC approximately. After that time, O_3 generated from precursors emitted by local sources appears, reaching contributions up to 15 and 12 ppb for urban and suburban locations (28 and 22% of the total ozone, respectively) around 12:00 UTC. The road transport (14-10%) and the residential (2-4%) sectors are those with the highest contributions. The signal of anthropogenic sources is lower in rural monitoring stations. As an average, road traffic contributes a maximum of 5% (5 ppb), the residential sector 2% (2 ppb) and the use of solvents (VOC emissions) also around 2%.

The results in Figure 11 demonstrate the persistent relevance of initial conditions in all locations, but especially in rural locations. Even though the initial conditions contribute to O_3 concentration throughout the day, the maximums values are found in the first hours (0:00 -5:00 UTC). As the day evolves, the influence from IC progressively decreases until they disappear at 21:00 UTC approximately. However, clear differences are found depending on the circulation pattern as illustrated for July 27th (accumulation) and July, 13th (advection). According to the model predictions, O_3 concentrations are greater during the accumulation period (and are reached slightly earlier), with maxima up to 68 ppb (17:00 UTC) in contrast with 52 ppb under advective conditions. Of note, the model is able to reproduce observed O_3 temporal patterns quite consistently, but it misses the peak values during accumulation periods (Table S4 and Table S5).

It may be highlighted that the influence of residual layers of the previous day is observed again at the central hours of the day is very significant under accumulation conditions (up to 12 ppb, around 18% of total of O_3) while is practically missing for advective days. This relates to the enhancement of O_3 levels from reservoirs aloft discussed in section 3.2.1. that does not occur under advective conditions. Of note, and consistently with the analysis in section 3.2, we observe that the contribution from local anthropogenic sources to O_3 peaks is higher both, in absolute and relative terms, for accumulation periods, up to 18 ppb and 32%, respectively as an average in urban locations (in contrast with 22% under advective conditions).

These results point out that the source apportionment under unfavorable circulation patterns significantly differs from that for average or advective conditions. Nonetheless, clear differences are found for individual stations depending on their location relative to the city center and prevailing winds. In the supplement (Figure S11 to Figure S13) a stratification of the same results by station type and geographical quadrant (Figure S10) and distance to Madrid is shown. For instance, urban locations within Madrid municipality in the NE direction for the 27th present much higher contributions from local sources that urban stations in the NW direction and further away from the metropolitan area (Figure S12). This variability suggests that the outcome of local measures may differ throughout the region and should be modeled under specific meteorological conditions and assesses specifically for each location of interest.

https://doi.org/10.5194/egusphere-2023-2056
Preprint. Discussion started: 6 October 2023

4. Conclusions

A high-resolution chemical-transport model has been used to investigate O_3 dynamics for a typical summer month (July 2016) in the Madrid Region. The model presents an acceptable performance and succeeds in reproducing the phenomena described in previous studies (Querol et al., 2018, Escudero et al., 2019), confirming that O_3 dynamics are conditioned by regional circulation patterns. The source apportionment analysis shows that O_3 levels are dominated by non-local contributions, representing around 70% of mean values across the region. Ozone reservoirs from previous days in the mid troposphere are also important to build up high concentrations in accumulation episodes. The analysis, however, points out that precursors emitted by local sources play a more important role regarding the highest concentration values, illustrated in this study by the 90^{th} percentile. This suggest that the implementation of emission reduction strategies in the region may be more effective to control O_3 concentration peaks than average values. This is particularly true under unfavorable, stagnation conditions associated with accumulation patterns where maxima O_3 concentrations occur. According to our results, up to 35% of total O_3 may be originated from local sources, giving a theoretical maximum reduction potential of 1-h values of approximately 25 ppb under these conditions. Among local sources, road traffic is the main contributor, accounting for 55% of local sources. Other relevant sectors are the residential, commercial and institutional sectors (non-industrial combustion sources) and the solvent use due to a significant share of VOCs emissions. At the same time, our results suggest that biogenic sources play a minor role (below 3% for the average O_3 concentration over the month), although they are responsible for 42.4% of total VOCs in the modeling domain.

We also found significant variations in source apportionment patterns across station types and relative locations. This implies that high-resolution simulations under specific meteorological conditions should be performed to anticipate the potential outcome on O_3 levels in different locations of the Madrid region.

Considering these results, future modeling efforts should be oriented to simulate the effect of specific measures both local and in cooperation with other administrations to identify optimal emission abatement strategies. The modeling platform used in this study may be also helpful to assess sensitivities to different factors, including sensitivity regimes or NO_X and VOCs speciation for specific sources.

Author contributions

RB and DP designed the research. DP and LT conducted the CMAQ modeling and data postprocessing. DP, JMA, LT, and RB analyzed the results. DP, RB and JMA wrote the paper with contributions from all authors. GS and SN provided support for the CMAQ model and reviewed the article.

Competing interests

The authors declare that they have no conflict of interest.

Disclaimer

The views expressed in this paper are those of the authors and do not necessarily represent the views or policies of the U.S. EPA.

Financial support

https://doi.org/10.5194/egusphere-2023-2056
Preprint. Discussion started: 6 October 2023

This study was carried out within AIRTEC-CM (urban air quality and climate change integral assessment) scientific program funded by the Directorate General for Universities and Research of the Greater Madrid Region (S2018/EMT-4329).

Acknowledgements

The authors gratefully acknowledge the Universidad Politécnica de Madrid (www.upm.es) for providing computing resources on Magerit Supercomputer.

References

AEMET.: Informe Anual 2016, Ministerio de Agricultura y Pesca, Alimentación y Medio Ambiente, https://www.aemet.es/documentos/es/conocenos/a_que_nos_dedicamos/informes/InformeAnualAEMET_2016_web.pdf, 2017.

AM.: Calidad del Aire Madrid 2022, https://www.madrid.es/UnidadesDescentralizadas/Sostenibilidad/EspeInf/Borrador%20Acci%C3%B3nClim%C3%A1tica/Planes%20e%20Inventarios/4aInventario/Ficheros/Inventario_emisiones_Ayto_Madrid_1999_a_2020.pdf, 2022.

Appel, K., Pouliot, G., Simon, H., Sarwar, G., Pye, H., Napelenok, S., Akhtar, F., and Roselle, S.: Evaluation of dust and trace metal estimates from the Community Multiscale Air Quality (CMAQ) model version 5.0, Geoscientific Model Development, 6, 883-899, https://doi.org/10.5194/gmd-6-883-2013, 2013.

Baek, B. H. and Seppanen, C.: Sparse Matrix Operator Kernel Emissions (SMOKE) Modeling System (Version SMOKE User's Documentation), http://doi.org/10.5281/zenodo.1421403, 2018.

Baker, K., Woody, M., Tonnesen, G., Hutzell, W., Pye, H., Beaver, M., Pouliot, G., and Pierce, T.: Contribution of regional-scale fire events to ozone and PM2. 5 air quality estimated by photochemical modeling approaches, Atmospheric Environment, 140, 539-554, https://doi.org/10.1016/j.atmosenv.2016.06.032, 2016.

Banerjee, A., Maycock, A. C., Archibald, A. T., Abraham, N. L., Telford, P., Braesicke, P., and Pyle, J. A.: Drivers of changes in stratospheric and tropospheric ozone between year 2000 and 2100, Atmospheric Chemistry and Physics, 16, 2727-2746, https://doi.org/10.5194/acp-16-2727-2016, 2016.

Bates, D., Bell, G., Burnham, C., Hazucha, M., Mantha, J., Pengelly, L., and Silverman, F.: Short-term effects of ozone on the lung, Journal of Applied Physiology, 32, 176-181, https://doi.org/10.1152/jappl.1972.32.2.176, 1972.

Bell, M. L., McDermott, A., Zeger, S. L., Samet, J. M., and Dominici, F.: Ozone and short-term mortality in 95 US urban communities, 1987-2000, Jama, 292, 2372-2378, https://doi.org/10.1001/jama.292.19.2372, 2004.

Borge, R., de la Paz, D., Cordero J.M., Sarwar, G., Napelenok, S.: Comparison of Source Apportionment Methods to attribute summer tropospheric O_3 and NO_2 levels in Madrid (Spain) 21st International Conference on Harmonisation within Atmospheric Dispersion Modelling for Regulatory Purposes. HARMO21, Aveiro, Portugal, 27-30 September 33-37

Borge, R., Lumbreras, J., and Rodríguez, E.: Development of a high-resolution emission inventory for Spain using the SMOKE modelling system: a case study for the years 2000 and 2010, Environmental Modelling & Software, 23, 1026-1044, https://doi.org/10.1016/j.envsoft.2007.11.002, 2008.

Borge, R., Jung, D., Lejarraga, I., de la Paz, D., and Cordero, J. M.: Assessment of the Madrid region air quality zoning based on mesoscale modelling and k-means clustering, Atmospheric Environment, 287, 119258, https://doi.org/10.1016/j.atmosenv.2022.119258, 2022.

Borge, R., López, J., Lumbreras, J., Narros, A., and Rodríguez, E.: Influence of boundary conditions on CMAQ simulations over the Iberian Peninsula, Atmospheric Environment, 44, 2681-2695, https://doi.org/10.1016/j.atmosenv.2010.04.044, 2010.

https://doi.org/10.5194/egusphere-2023-2056
Preprint. Discussion started: 6 October 2023

Borge, R., Requia, W. J., Yagüe, C., Jhun, I., and Koutrakis, P.: Impact of weather changes on air quality and related mortality in Spain over a 25 year period [1993–2017], Environment international, 133, 105272, https://doi.org/10.1016/j.envint.2019.105272, 2019.

Borge, R., Lumbreras, J., Pérez, J., de la Paz, D., Vedrenne, M., de Andrés, J. M., and Rodríguez, M. E.: Emission inventories and modeling requirements for the development of air quality plans. Application to Madrid (Spain), Science of the Total Environment, 466-467, 809-819, https://doi.org/10.1016/j.scitotenv.2013.07.093, 2014.

Borge, R., Santiago, J. L., Paz, D. d. l., Martín, F., Domingo, J., Valdes, C., Sanchez, B., Rivas, E., Rozas, M. T., Lázaro, S., Perez, J., and Fernandez, A.: Application of a short term air quality action plan in Madrid (Spain) under a high-pollution episode -Part II: Assessment from multi-scale modelling, https://doi.org/10.1016/j.scitotenv.2018.04.323, 2018.

Brodin, M., Helmig, D., and Oltmans, S.: Seasonal ozone behavior along an elevation gradient in the Colorado Front Range Mountains, Atmospheric Environment, 44, 5305-5315, https://doi.org/10.1016/j.atmosenv.2010.06.033, 2010.

Brook, J., Makar, P., Sills, D., Hayden, K., and McLaren, R.: Exploring the nature of air quality over southwestern Ontario: main findings from the Border Air Quality and Meteorology Study, Atmospheric Chemistry and Physics, 13, 10461-10482, https://doi.org/10.5194/acp-13-10461-2013, 2013.

Byun, D. and Schere, K. L.: Review of the governing equations, computational algorithms, and other components of the Models-3 Community Multiscale Air Quality (CMAQ) modeling system, Applied Mechanics Reviews, 59, 51-77, https://doi.org/10.1115/1.2128636, 2006.

Carnero, J. A. A., Bolívar, J. P., and Benito, A.: Surface ozone measurements in the southwest of the Iberian Peninsula (Huelva, Spain), Environmental Science and Pollution Research, 17, 355-368, https://doi.org/10.1007/s11356-008-0098-9, 2010.

Ching, J. and Byun, D.: Introduction to the Models-3 framework and the Community Multiscale Air Quality model (CMAQ), Science Algorithms of the EPA Models-3 Community Multiscale Air Quality (CMAQ) Modeling System, https://www.cmascenter.org/cmaq/science_documentation/pdf/ch01.pdf (last access: 21 November 2022), 1999.

CM: Inventario de emisiones a la atmósfera en la Comunidad de Madrid. Años 1990-2018, Comunidad de Madrid. Dirección General de Sostenibilidad y Cambio Climático, https://www.comunidad.madrid/sites/default/files/doc/medio-ambiente/documento_de_sintesis_inventario_de_emisiones_comunidad_de_madrid.pdf (last access: 14 August 2022), 2021.

Cohan, D. S. and Napelenok, S. L.: Air quality response modeling for decision support, Atmosphere, 2, 407-425, https://doi.org/10.3390/atmos2030407, 2011.

Collet, S., Kidokoro, T., Karamchandani, P., Jung, J., and Shah, T.: Future year ozone source attribution modeling study using CMAQ-ISAM, Journal of the Air & Waste Management Association, 68, 1239-1247, https://doi.org/10.1080/10962247.2018.1496954, 2018.

De Andrés, J. M., Borge, R., De La Paz, D., Lumbreras, J., and Rodríguez, E.: Implementation of a module for risk of ozone impacts assessment to vegetation in the Integrated Assessment Modelling system for the Iberian Peninsula. Evaluation for wheat and Holm oak, Environmental Pollution, 165, 25-37, https://doi.org/10.1016/j.envpol.2012.01.048, 2012.

de la Paz, D., Borge, R., Perez, J., de Andrés, J.M.: Contributions to summer ground-level O_3 in the Madrid Region. Proceedings of Abstracts of the 12th International Conference on Air Quality Science and Application (18-22 May 2020) p. 153, https://doi.org/10.18745/PB.22217, 2020.

EEA.: Air quality in europe 2020 report, European Environment Agency, https://doi.org/10.2800/786656, 2020.

EEA.: European Union emission inventory report 1990-2020 Under the UNECE Air Convention European Environment Agency, Luxembourg: Publications Office of the European Union, 2022, https://doi.org/10.2800/928370, 2022

Emery, C., Jung, J., Koo, B., and Yarwood, G.: Final Reprot, Improvements to CAMx Snow Cover Treatments and Carbon Bond Chemical Mechanism for Winter Ozone, Tech. rep., Ramboll Environ, https://www.camx.com/files/emaq4-07_task7_techmemo_r1_1aug16.pdf, 2015

https://doi.org/10.5194/egusphere-2023-2056
Preprint. Discussion started: 6 October 2023

Escudero, M., Segers, A., Kranenburg, R., Querol, X., Alastuey, A., Borge, R., De la Paz, D., Gangoiti, G., and Schaap, M.: Analysis of summer O_3 in the Madrid air basin with the LOTOS-EUROS chemical transport model, Atmospheric Chemistry and Physics, 19, 14211-14232, https://doi.org/10.5194/acp-19-14211-2019, 2019.

García, R., Prieto, L., Díaz, J., Hernández, E., and Del Teso, T.: Synoptic conditions leading to extremely high temperatures in Madrid, Annales Geophysicae, 237-245, https://doi.org/10.5194/ANGEO-20-237-2002, 2002.

Garrido-Pérez, J. M., Ordóñez, C., García-Herrera, R., and Schnell, J. L.: The differing impact of air stagnation on near-surface ozone across Europe, EGU General Assembly Conference Abstracts, 9213, https://doi.org/10.5194/egusphere-egu2020-9213, 2020.

Gaudel, A., Cooper, O., Ancellet, G., Barret, B., Boynard, A., Burrows, J., Clerbaux, C., Coheur, P.-F., Cuesta, J., and Cuevas Agulló, E.: Tropospheric Ozone Assessment Report: Present-day distribution and trends of tropospheric ozone relevant to climate and global atmospheric chemistry model evaluation, https://doi.org/10.1525/elementa.291, 2018.

Goodman, J. E., Zu, K., Loftus, C. T., Lynch, H. N., Prueitt, R. L., Mohar, I., Shubin, S. P., and Sax, S. N.: Short-term ozone exposure and asthma severity: Weight-of-evidence analysis, Environmental research, 160, 391-397, https://doi.org/10.1016/j.envres.2017.10.018, 2018.

Granados-Muñoz, M. J. and Leblanc, T.: Tropospheric ozone seasonal and long-term variability as seen by lidar and surface measurements at the JPL-Table Mountain Facility, California, Atmospheric Chemistry and Physics, 16, 9299-9319, https://doi.org/10.5194/acp-16-9299-2016, 2016.

Guenther, A. B., Jiang, X., Heald, C. L., Sakulyanontvittaya, T., Duhl, T., Emmons, L. K., and Wang, X.: The Model of Emissions of Gases and Aerosols from Nature version 2.1 (MEGAN2.1): an extended and updated framework for modeling biogenic emissions, Geosci. Model Dev., 5, https://doi.org/10.5194/gmd-5-1471-2012, 2012.

Guenther, C.: Estimates of global terrestrial isoprene emissions using MEGAN (Model of Emissions of Gases and Aerosols from Nature), Atmospheric Chemistry and Physics, 6, https://doi.org/10.5194/acp-6-3181-2006, 2006.

Han, X., Zhu, L., Wang, S., Meng, X., Zhang, M., and Hu, J.: Modeling study of impacts on surface ozone of regional transport and emissions reductions over North China Plain in summer 2015, Atmospheric Chemistry and Physics, 18, 12207-12221, https://doi.org/10.5194/acp-18-12207-2018, 2018.

Harmens, H., Mills, G., Hayes, F., and Norris, D.: Air pollution and vegetation: ICP Vegetation annual report 2010/2011, ISBN: 978-1-906698-26-3, 2011.

Hsu, J., Prather, M. J., and Wild, O.: Diagnosing the stratosphere-to-troposphere flux of ozone in a chemistry transport model, Journal of Geophysical Research: Atmospheres, 110, https://doi.org/10.1029/2005JD006045, 2005.

Hsu, Y., Strait, R., Roe, S., and Holoman, D.: SPECIATE 4.0 Speciation database development documentation: Final Report, EPA/600/R-06/161 US Environmental Protection Agency, Office of Research and and Development U.S. Environmental Protection Agency Research Triangle Park, NC 27711, https://cfpub.epa.gov/si/si_public_file_download.cfm?p_download_id=459904&Lab=NRMRL, 2006.

University of North Carolina at Chapel Hill (UNC):SMOKE's V365 User's Manual, https://www.cmascenter.org/smoke/documentation/3.6.5/manual_smokev365.pdf, 2015

IPCC: Working Group I: The physical science basis, Projections of Future Changes in Climate: http://www.ipcc.ch/publications_and_data/ar4/wg1/en/spmsspm-projections-of.Html, 2007.

IPCC: Climate change 2014: mitigation of climate change, Cambridge University Press, ISBN 978-1-107-05821-7, 2015.

Jenkin, M. E. and Clemitshaw, K. C.: Ozone and other secondary photochemical pollutants: chemical processes governing their formation in the planetary boundary layer, Atmospheric Environment, 34, 2499-2527, https://doi.org/10.1016/S1352-2310(99)00478-1, 2000.

https://doi.org/10.5194/egusphere-2023-2056
Preprint. Discussion started: 6 October 2023

Jerrett, M., Burnett, R. T., Pope III, C. A., Ito, K., Thurston, G., Krewski, D., Shi, Y., Calle, E., and Thun, M.: Long-term ozone exposure and mortality, New England Journal of Medicine, 360, 1085-1095, https://doi.org/10.1056/NEJMoa0803894, 2009.

Jhun, I., Coull, B. A., Zanobetti, A., and Koutrakis, P.: The impact of nitrogen oxides concentration decreases on ozone trends in the USA, Air Quality, Atmosphere & Health, 8, 283-292, https://doi.org/10.1007/s11869-014-0279-2, 2015.

Jung, D., de la Paz, D., Notario, A., and Borge, R.: Analysis of emissions-driven changes in the oxidation capacity of the atmosphere in Europe, Science of The Total Environment, 827, 154126, https://doi.org/10.1016/j.scitotenv.2022.154126, 2022.

Li, X., Qin, M., Li, L., Gong, K., Shen, H., Li, J., and Hu, J.: Examining the implications of photochemical indicators for O 3–NO x–VOC sensitivity and control strategies: a case study in the Yangtze River Delta (YRD), China, Atmospheric Chemistry and Physics, 22, 14799-14811, https://doi.org/10.5194/acp-22-14799-2022, 2022.

Logan, J. A.: Tropospheric ozone: Seasonal behavior, trends, and anthropogenic influence, Journal of Geophysical Research: Atmospheres, 90, 10463-10482, https://doi.org/10.1029/JD090iD06p10463, 1985.

Massagué, J., Escudero, M., Alastuey, A., Mantilla, E., Monfort, E., Gangoiti, G., García-Pando, C. P., and Querol, X.: Spatiotemporal variations of tropospheric ozone in Spain (2008–2019), Environment International, 176, 107961, https://doi.org/10.1016/j.envint.2023.107961, 2023.

Mathur, R., Xing, J., Gilliam, R., Sarwar, G., Hogrefe, C., Pleim, J., Pouliot, G., Roselle, S., Spero, T. L., and Wong, D. C.: Extending the Community Multiscale Air Quality (CMAQ) modeling system to hemispheric scales: overview of process considerations and initial applications, Atmospheric chemistry and physics, 17, 12449-12474, https://doi.org/10.5194/acp-17-12449-2017, 2017.

Meul, S., Langematz, U., Kröger, P., Oberländer-Hayn, S., and Jöckel, P.: Future changes in the stratosphere-to-troposphere ozone mass flux and the contribution from climate change and ozone recovery, Atmospheric Chemistry and Physics, 18, 7721-7738, https://doi.org/10.5194/acp-18-7721-2018, 2018.

Millan, M. M., Mantilla, E., Salvador, R., Carratalá, A., Sanz, M. J., Alonso, L., Gangoiti, G., and Navazo, M.: Ozone cycles in the western Mediterranean basin: interpretation of monitoring data in complex coastal terrain, Journal of Applied Meteorology, 39, 487-508, https://doi.org/10.1175/1520-0450(2000)039<0487:OCITWM>2.0.CO;2, 2000.

Mills, G., Pleijel, H., Braun, S., Büker, P., Bermejo, V., Calvo, E., Danielsson, H., Emberson, L., Fernández, I. G., and Grünhage, L.: New stomatal flux-based critical levels for ozone effects on vegetation, Atmospheric Environment, 45, 5064-5068, https://doi.org/10.1016/j.atmosenv.2011.06.009, 2011.

Millán, M., Artíñano, B., Alonso, L., Navazo, M., and Castro, M.: The effect of meso-scale flows on regional and long-range atmospheric transport in the western Mediterranean area, Atmospheric environment. part a. general topics, 25, 949-963, https://doi.org/10.1016/0960-1686(91)90137-V, 1991.

MMA : Inventario Nacional de contaminantes atmosféricos, https://unfccc.int/resource/podcast/nir/ES_NIR_UNFCCC_2018.pdf 2018.

Monks, P. S., Archibald, A., Colette, A., Cooper, O., Coyle, M., Derwent, R., Fowler, D., Granier, C., Law, K. S., and Mills, G.: Tropospheric ozone and its precursors from the urban to the global scale from air quality to short-lived climate forcer, https://doi.org/10.5194/acp-15-8889-2015, 2015.

Napelenok, S.: Description of the ISAM Chemistry Method, https://github.com/USEPA/CMAQ/blob/main/DOCS/Users_Guide/CMAQ_UG_ch11_ISAM.md, 2020a

Napelenok, S., Bill Hutzell, C. Hogrefe, B. Murphy, J. Bash, K. Baker, K. Foley, Q. Shu, AND R. Mathur. CMAQ 5.3.2: Updates to Integrated Source Apportionment Method (ISAM). CMAS Annual Conference 2020, Chapel Hill, NC, October 19 - 21, https://youtu.be/959lYeSeEf4, 2020b

https://doi.org/10.5194/egusphere-2023-2056
Preprint. Discussion started: 6 October 2023

Nguyen, D.-H., Lin, C., Vu, C.-T., Cheruiyot, N. K., Nguyen, M. K., Le, T. H., Lukkhasorn, W., and Bui, X.-T.: Tropospheric ozone and NOx: a review of worldwide variation and meteorological influences, Environmental Technology & Innovation, 102809, https://doi.org/10.1016/j.eti.2022.102809, 2022.

Paoletti, E., De Marco, A., Beddows, D. C., Harrison, R. M., and Manning, W. J.: Ozone levels in European and USA cities are increasing more than at rural sites, while peak values are decreasing, Environmental Pollution, 192, 295-299, https://doi.org/10.1016/j.envpol.2014.04.040, 2014.

Pay, M. T., Gangoiti, G., Guevara, M., Napelenok, S., Querol, X., Jorba, O., and Pérez García-Pando, C.: Ozone source apportionment during peak summer events over southwestern Europe, Atmospheric Chemistry and Physics, 19, https://doi.org/10.5194/acp-19-5467-2019, 2019.

Plaza, J., Pujadas, M., and Artíñano, B.: Formation and transport of the Madrid ozone plume, Journal of the Air & Waste Management Association, 47, 766-774, https://doi.org/10.1080/10473289.1997.10463938, 1997.

Qu, Z., Wu, D., Henze, D. K., Li, Y., Sonenberg, M., and Mao, F.: Transboundary transport of ozone pollution to a US border region: A case study of Yuma, Environmental Pollution, 273, 116421, https://doi.org/10.1016/j.envpol.2020.116421, 2021.

Quaassdorff, C., Borge, R., Pérez, J., Lumbreras, J., de la Paz, D., and de Andrés, J. M.: Microscale traffic simulation and emission estimation in a heavily trafficked roundabout in Madrid (Spain), Science of the Total Environment, 566, 416-427, https://doi.org/10.1016/j.scitotenv.2016.05.051, 2016.

Querol, X., Alastuey, A., Gangoiti, G., Perez, N., Lee, H. K., Eun, H. R., Park, Y., Mantilla, E., Escudero, M., and Titos, G.: Phenomenology of summer ozone episodes over the Madrid Metropolitan Area, central Spain, Atmospheric Chemistry and Physics, 18, 6511-6533, https://doi.org/10.5194/acp-18-6511-2018, 2018.

Querol, X., Alastuey, A., Pandolfi, M., Reche, C., Pérez, N., Minguillón, M. C., Moreno, T., Viana, M., Escudero, M., and Orio, A.: 2001–2012 trends on air quality in Spain, Science of the Total Environment, 490, 957-969, https://doi.org/10.1016/j.scitotenv.2014.05.074, 2014.

Querol, X., Alastuey, A., Reche, C., Orio, A., Pallares, M., Reina, F., Dieguez, J., Mantilla, E., Escudero, M., and Alonso, L.: On the origin of the highest ozone episodes in Spain, Science of the Total Environment, 572, 379-389, https://doi.org/10.1016/j.scitotenv.2016.07.193, 2016.

Otte, T. L. and Pleim, J. E.: The Meteorology-Chemistry Interface Processor (MCIP) for the CMAQ modeling system: updates through MCIPv3.4.1, Geosci. Model Dev., 3, 243–256, https://doi.org/10.5194/gmd-3-243-2010, 2010

Querol, X., Gangoiti, G., Mantilla, E., Alastuey, A., Minguillón, M. C., Amato, F., Reche, C., Viana, M., Moreno, T., and Karanasiou, A.: Phenomenology of high-ozone episodes in NE Spain, Atmospheric Chemistry and Physics, 17, https://doi.org/doi:10.5194/acp-17-2817-2017, 2017.

Reche, C., Moreno, T., Amato, F., Pandolfi, M., Pérez, J., de La Paz, D., Diaz, E., Gómez-Moreno, F., Pujadas, M., and Artíñano, B.: Spatio-temporal patterns of high summer ozone events in the Madrid Basin, Central Spain, Atmospheric Environment, 185, 207-220, https://doi.org/10.1016/j.atmosenv.2018.05.002, 2018.

Saiz-Lopez, A., Borge, R., Notario, A., Adame, J. A., Paz, D. D. L., Querol, X., Artíñano, B., Gómez-Moreno, F. J., and Cuevas, C. A.: Unexpected increase in the oxidation capacity of the urban atmosphere of Madrid, Spain, Scientific Reports, 7, http://doi.org/10.1038/srep45956, 2017.

Sarwar, G., Simon, H., Bhave, P., and Yarwood, G.: Examining the impact of heterogeneous nitryl chloride production on air quality across the United States, Atmospheric Chemistry and Physics, 12, 6455-6473, https://doi.org/10.5194/acp-12-6455-2012, 2012.

Seinfeld, J. H. and Pandis, S. N.: Atmospheric chemistry and physics: from air pollution to climate change, John Wiley & Sons, ISBN: 978-1-118-94740-1, 2016.

https://doi.org/10.5194/egusphere-2023-2056
Preprint. Discussion started: 6 October 2023

Seltzer, K. M., Shindell, D. T., and Malley, C. S.: Measurement-based assessment of health burdens from long-term ozone exposure in the United States, Europe, and China, Environmental Research Letters, 13, https://doi.org/10.1088/1748-9326/aae29d, 2018.

Sicard, P., Agathokleous, E., Anenberg, S. C., De Marco, A., Paoletti, E., and Calatayud, V.: Trends in urban air pollution over the last two decades: A global perspective, Science of The Total Environment, 858, 160064, https://doi.org/10.1016/j.scitotenv.2022.160064, 2023.

Simon, H., Valin, L. C., Baker, K. R., Henderson, B. H., Crawford, J. H., Pusede, S. E., Kelly, J. T., Foley, K. M., Chris Owen, R., and Cohen, R. C.: Characterizing CO and NOy sources and relative ambient ratios in the Baltimore area using ambient measurements and source attribution modeling, Journal of Geophysical Research: Atmospheres, 123, 3304-3320, https://doi.org/10.1002/2017JD027688, 2018.

Sitch, S., Cox, P., Collins, W., and Huntingford, C.: Indirect radiative forcing of climate change through ozone effects on the land-carbon sink, Nature, 448, 791, https://doi.org/10.1038/nature06059, 2007.

Skamarock, W. C. and Klemp, J. B.: A time-split nonhydrostatic atmospheric model for weather research and forecasting applications, Journal of Computational Physics, 227, 3465-3485, https://doi.org/10.1016/j.jcp.2007.01.037, 2008.

Stevenson, D., Dentener, F., Schultz, M., Ellingsen, K., Van Noije, T., Wild, O., Zeng, G., Amann, M., Atherton, C., and Bell, N.: Multimodel ensemble simulations of present-day and near-future tropospheric ozone, Journal of Geophysical Research: Atmospheres, 111, https://doi.org/10.1029/2005JD006338, 2006.

Stocker, T. F., Qin, D., Plattner, G.-K., Tignor, M., Allen, S. K., Boschung, J., Nauels, A., Xia, Y., Bex, V., and Midgley, P. M.: Climate change 2013: The physical science basis, https://www.ipcc.ch/site/assets/uploads/2018/02/WG1AR5_all_final.pdf, 2013.

Thunis, P., Clappier, A., Tarrasón, L., Cuvelier, C., Monteiro, A., Pisoni, E., Wesseling, J., Belis, C., Pirovano, G., and Janssen, S.: Source apportionment to support air quality planning: Strengths and weaknesses of existing approaches, Environment international, 130, 104825, https://doi.org/10.1016/j.envint.2019.05.019, 2019.

Valverde, V., Pay, M. T., and Baldasano, J. M.: Ozone attributed to Madrid and Barcelona on-road transport emissions: Characterization of plume dynamics over the Iberian Peninsula, Science of the total environment, 543, 670-682, https://doi.org/10.1016/j.scitotenv.2015.11.070, 2016.

Whitten, G. Z., Heo, G., Kimura, Y., McDonald-Buller, E., Allen, D. T., Carter, W. P., and Yarwood, G.: A new condensed toluene mechanism for Carbon Bond: CB05-TU, Atmospheric Environment, 44, 5346-5355, https://doi.org/10.1016/j.atmosenv.2009.12.029, 2010.

WHO: WHO global air quality guidelines: particulate matter (PM2. 5 and PM10), ozone, nitrogen dioxide, sulfur dioxide and carbon monoxide: executive summary, ISBN:9789240034228 2021.

Xu, J., Ma, J., Zhang, X., Xu, X., Xu, X., Lin, W., Wang, Y., Meng, W., and Ma, Z.: Measurements of ozone and its precursors in Beijing during summertime: impact of urban plumes on ozone pollution in downwind rural areas, Atmospheric Chemistry and Physics, 11, 12241-12252, https://doi.org/10.5194/acp-11-12241-2011, 2011.

Yarwood, G., Jung, J., Whitten, G., Heo, G., J, M., and M, E.: Updates to the Carbon Bond Mechanism for Version 6 (CB6), in: 9th Annual CMAS Conference, pp. 1–4, Chapel Hill, NC, 2010

Young, P., Archibald, A., Bowman, K., Lamarque, J.-F., Naik, V., Stevenson, D., Tilmes, S., Voulgarakis, A., Wild, O., and Bergmann, D.: Pre-industrial to end 21st century projections of tropospheric ozone from the Atmospheric Chemistry and Climate Model Intercomparison Project (ACCMIP), Atmospheric Chemistry and Physics, 13, 2063-2090, https://doi.org/10.5194/acp-13-2063-2013, 2013.

Zaveri, R. A., Berkowitz, C. M., Kleinman, L. I., Springston, S. R., Doskey, P. V., Lonneman, W. A., and Spicer, C. W.: Ozone production efficiency and NOx depletion in an urban plume: Interpretation of field observations and implications for

https://doi.org/10.5194/egusphere-2023-2056
Preprint. Discussion started: 6 October 2023

evaluating O_3-NO_x-VOC sensitivity, Journal of Geophysical Research: Atmospheres, 108, https://doi.org/10.1029/2002JD003144, 2003.

Zhang, T., Xu, X., and Su, Y.: Impacts of Regional Transport and Meteorology on Ground-Level Ozone in Windsor, Canada, Atmosphere, 11, 1111, https://doi.org/10.3390/atmos11101111, 2020.

Ziemke, J. R., Oman, L. D., Strode, S. A., Douglass, A. R., Olsen, M. A., McPeters, R. D., Bhartia, P. K., Froidevaux, L., Labow, G. J., and Witte, J. C.: Trends in global tropospheric ozone inferred from a composite record of TOMS/OMI/MLS/OMPS satellite measurements and the MERRA-2 GMI simulation, Atmospheric Chemistry and Physics, 19, 3257-3269, https://doi.org/10.5194/acp-19-3257-2019, 2019.

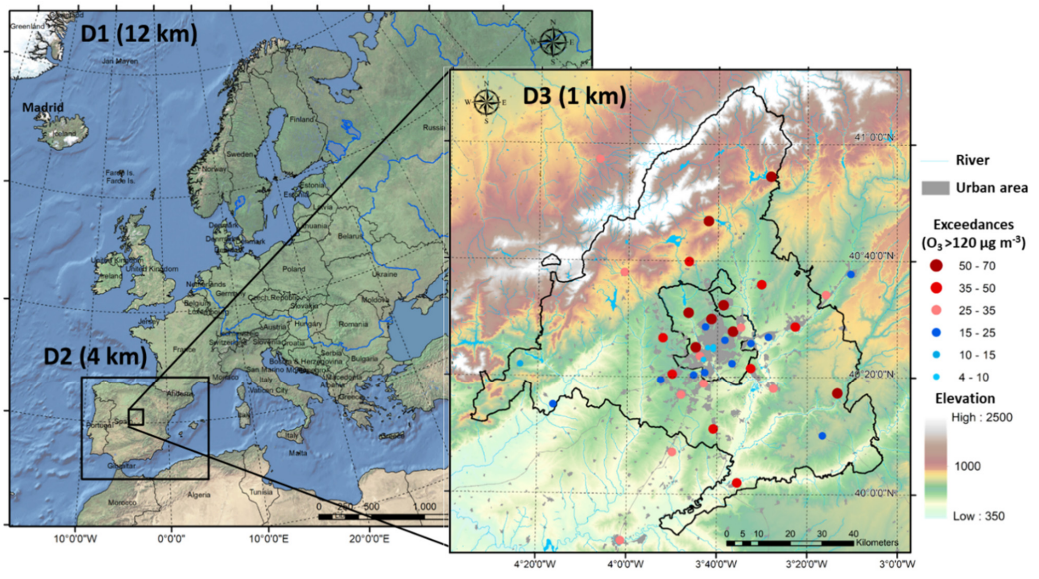

Figure. 1. Modeling domains including the location of the air quality monitoring stations within the innermost domain and number of exceedances of the O_3 target value for protection of human health (MDA8 > 120 µg·m^{-3}) in 2016.

https://doi.org/10.5194/egusphere-2023-2056
Preprint. Discussion started: 6 October 2023

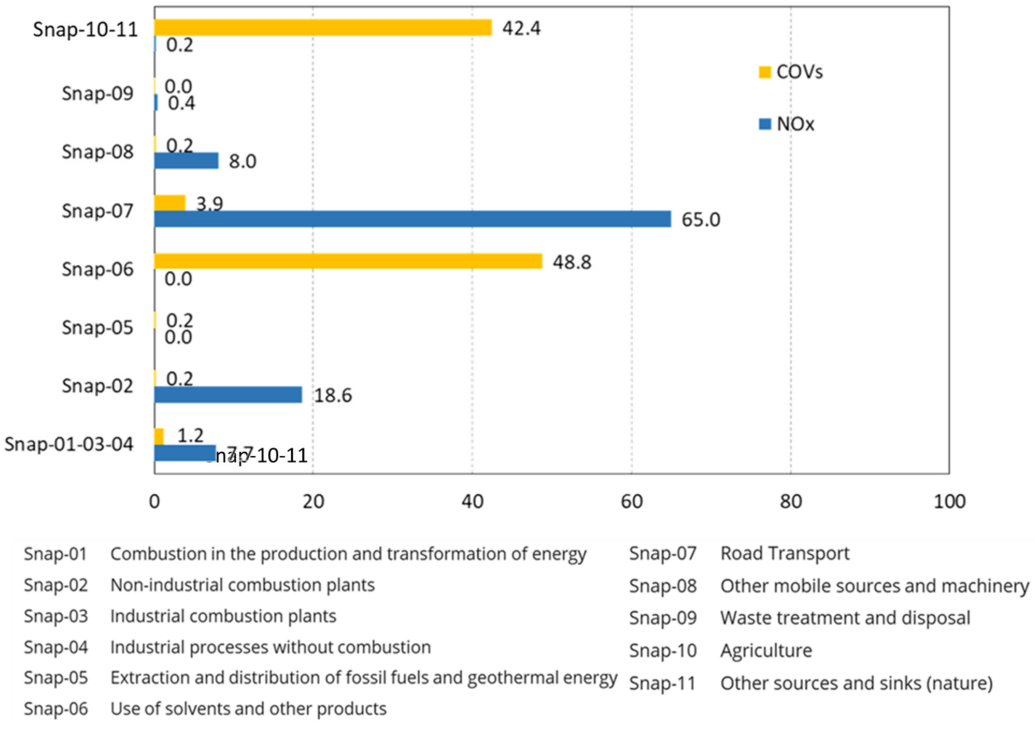

Figure. 2. NO_X and VOCs emissions of tagged sectors (annual) for the source apportionment analysis.

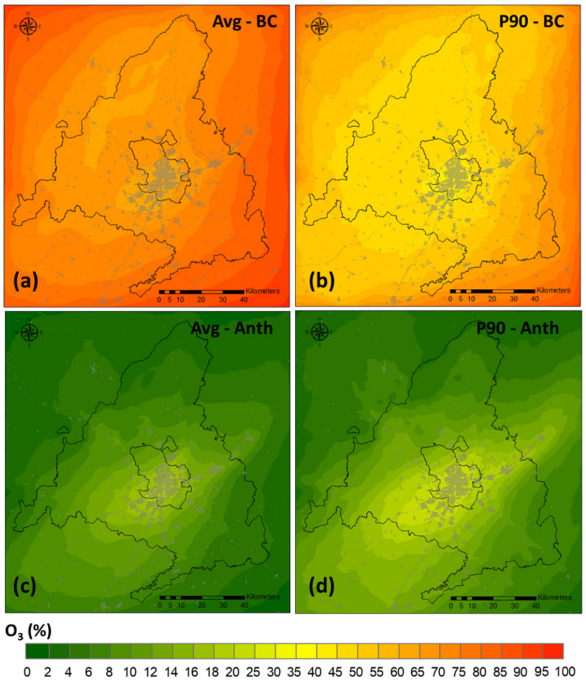

Figure. 3. Contribution (%) of BC to O_3 concentration: (a) monthly average and (b) 90th percentile. Contribution (%) of local anthropogenic emissions to (c) monthly average and (d) 90th percentile.

https://doi.org/10.5194/egusphere-2023-2056
Preprint. Discussion started: 6 October 2023

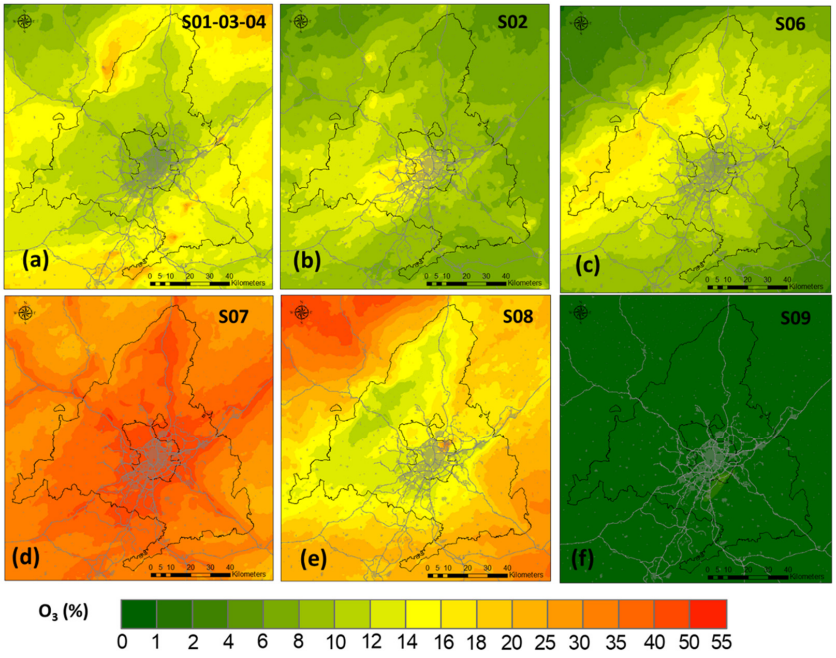

Figure 4. Percentage contribution to the 90th percentile of O_3 concentration of the main emitting sectors with respect to the total anthropogenic contribution.

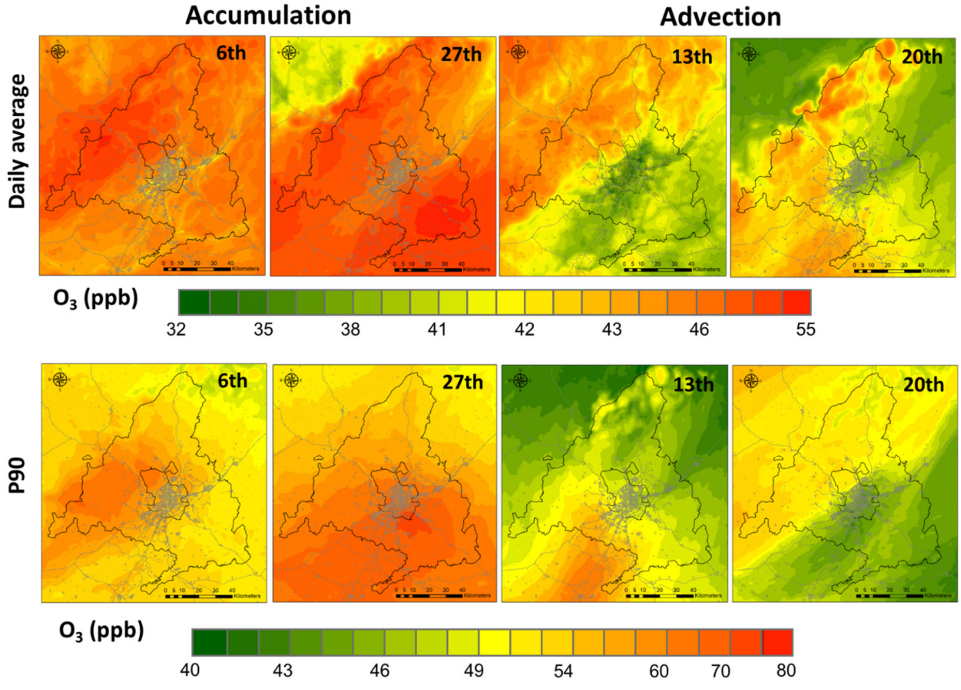

620 **Figure 5. Daily mean (top) and 90th percentile (bottom) of O_3 concentration (ppb) during accumulation (6th and 27th July, 2016) and advective (13th and 20th July, 2016) periods**

https://doi.org/10.5194/egusphere-2023-2056
Preprint. Discussion started: 6 October 2023

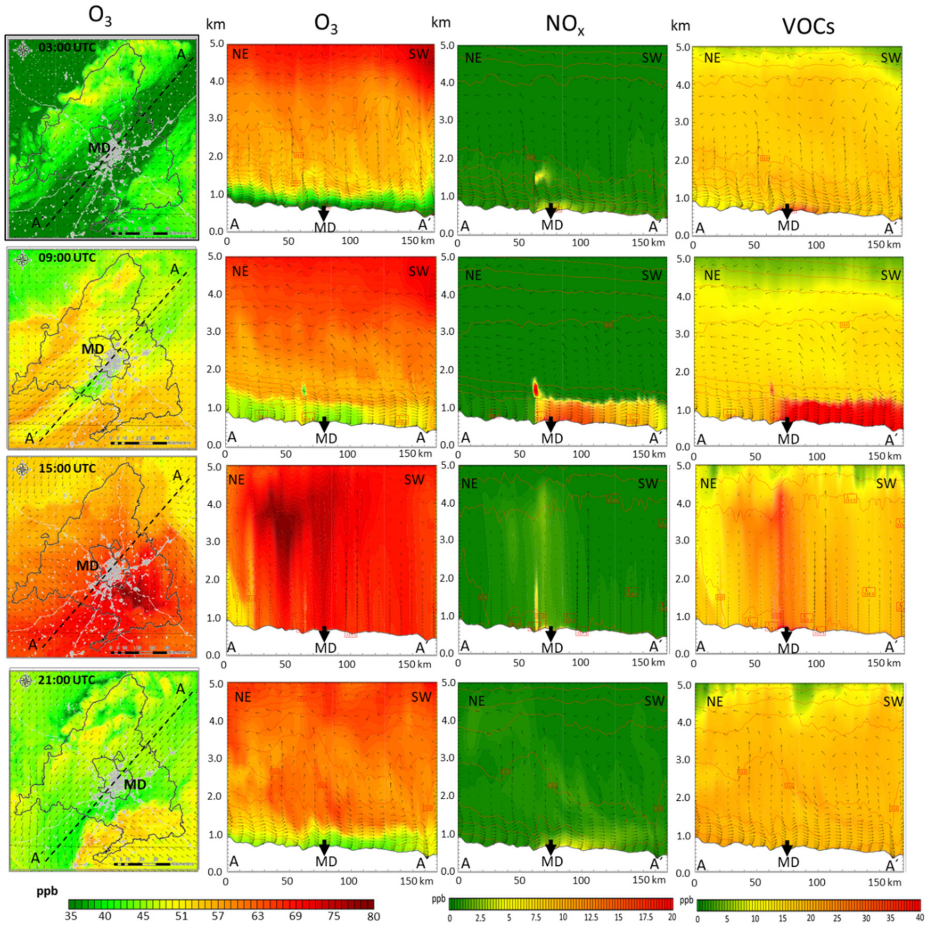

Figure 6. Accumulation period: hourly concentration during July 27th, 2016. From left to right, plan view and NE-SW cross section (up to 5 km height) O_3 concentrations (ppb), NOx (ppb) and VOCs (ppb) at the 3:00, 9:00; 15:00, 21: 00 UTC hours. MD = Madrid City.

https://doi.org/10.5194/egusphere-2023-2056
Preprint. Discussion started: 6 October 2023

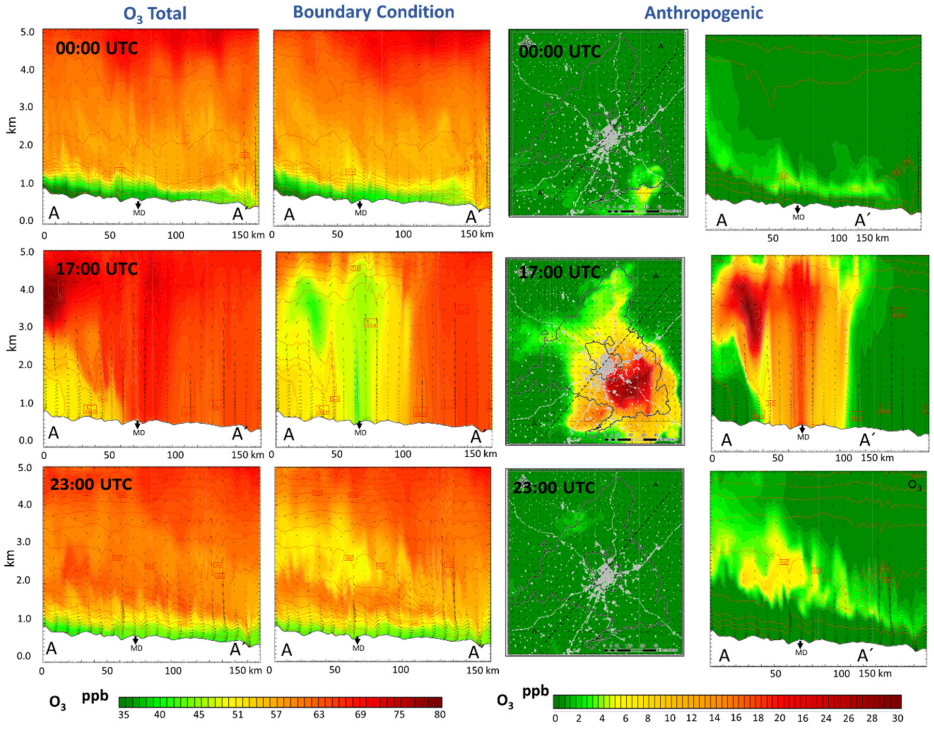

Figure 7. Hourly O_3 concentration profiles (at 0:00, 17:00; 23:00 UTC) for the NE-SW cross section and contribution of BC and anthropogenic local emissions on July 27th, 2016 (accumulation). MD = Madrid City.

https://doi.org/10.5194/egusphere-2023-2056
Preprint. Discussion started: 6 October 2023

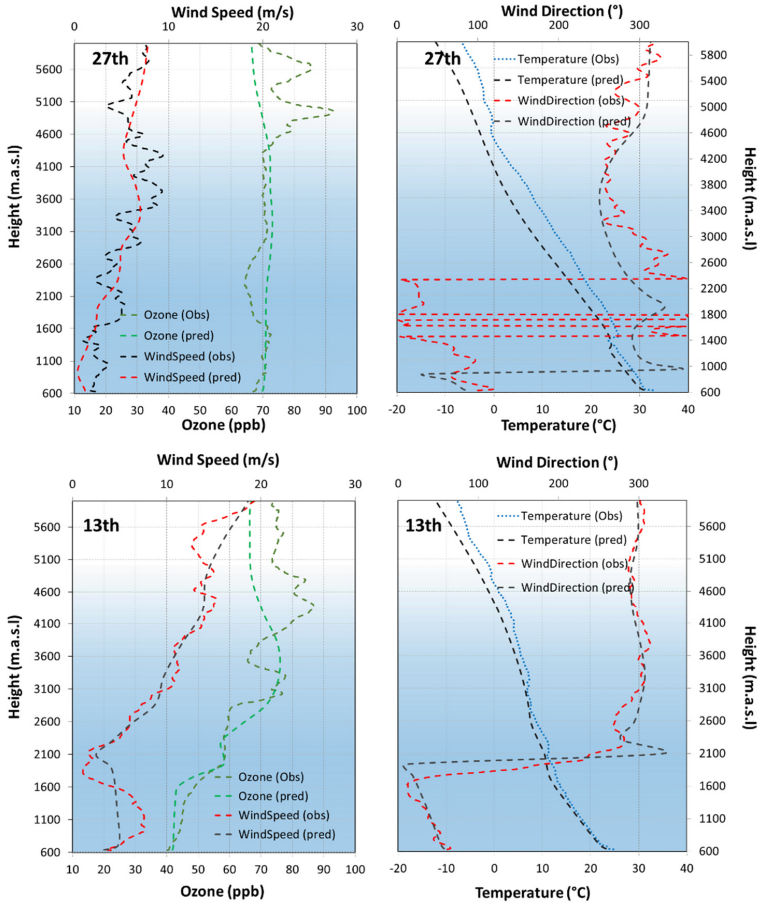

630 **Figure 8. Vertical profiles (noon UTC) of O_3, temperature, wind speed and wind direction for July 27th (accumulation, up) and the July13th (advective, down).**

https://doi.org/10.5194/egusphere-2023-2056
Preprint. Discussion started: 6 October 2023

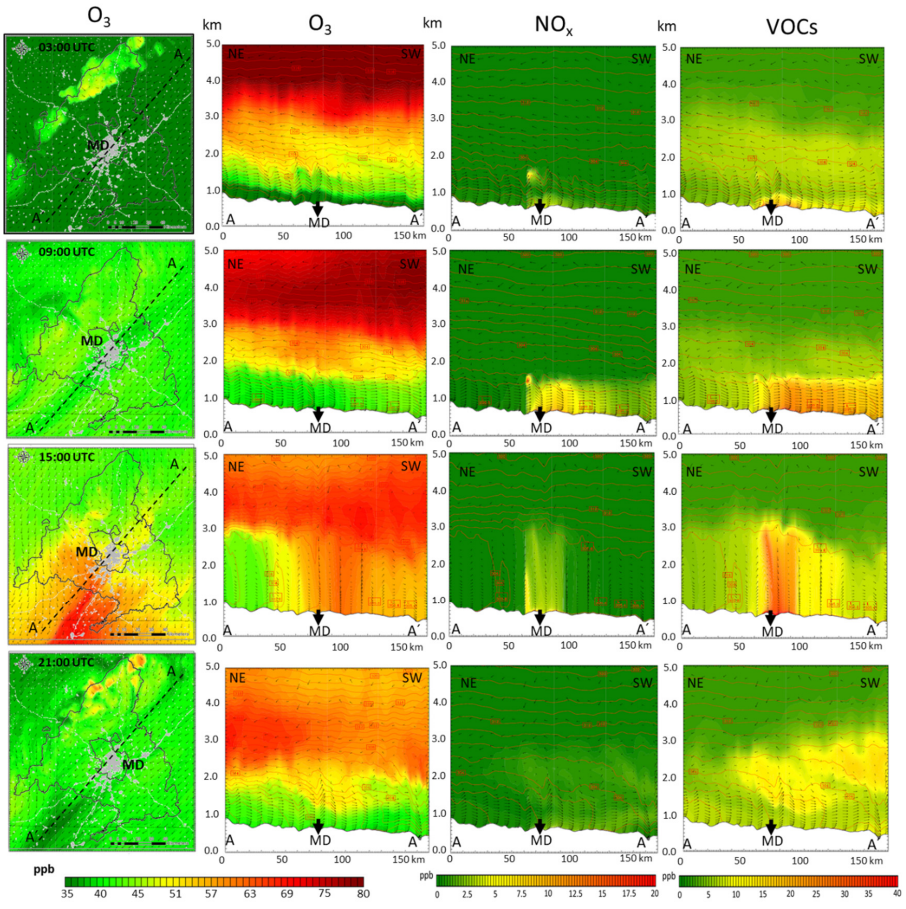

Figure 9. Advective period: hourly concentration during July 13th, 2016. From left to right, plan view and NE-SW cross section (up to 5 km height) O_3 concentrations (ppb), NOx (ppb) and VOCs (ppb) at the 3:00, 9:00; 15:00, 21: 00 UTC hours. MD = Madrid City.

https://doi.org/10.5194/egusphere-2023-2056
Preprint. Discussion started: 6 October 2023

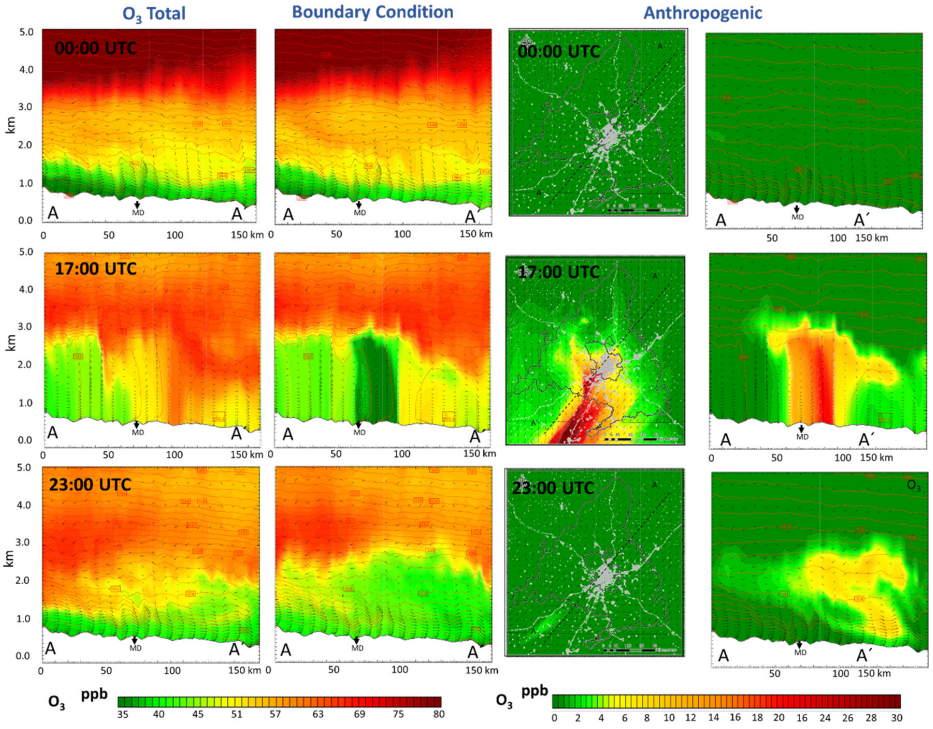

Figure 10. Hourly O_3 concentration profiles (at 0:00, 17:00; 23:00 UTC) for the NE-SW cross section and contribution of BC and anthropogenic local emissions on July 13th, 2016 (advection). MD = Madrid City.

640

https://doi.org/10.5194/egusphere-2023-2056
Preprint. Discussion started: 6 October 2023

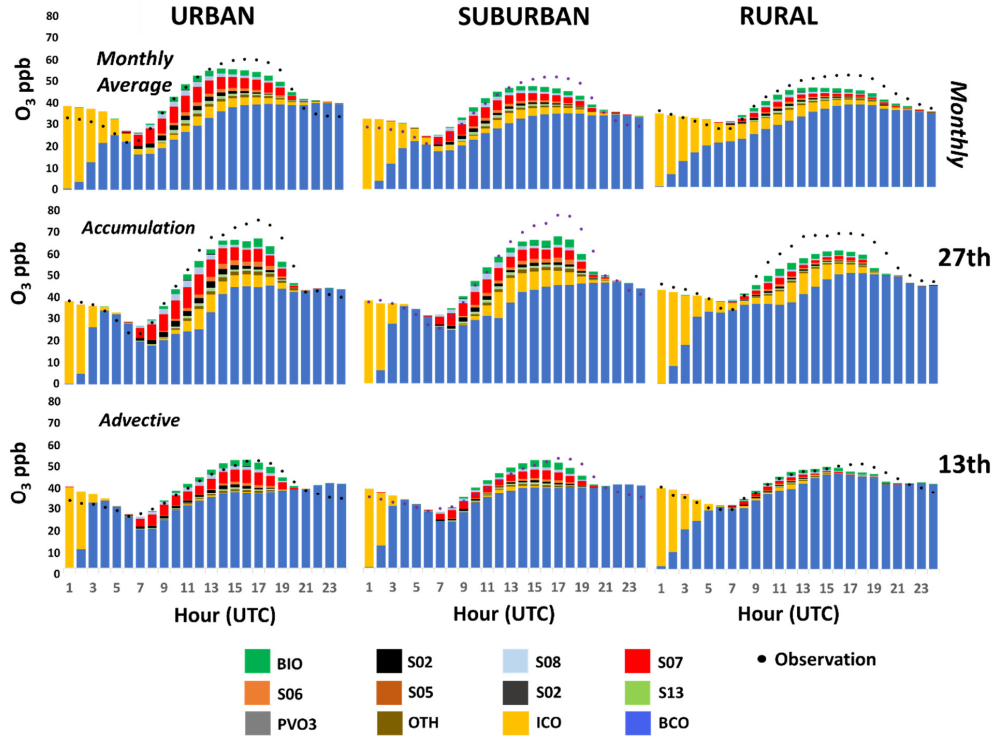

Figure 11. Hourly contribution for the monthly average (top) and specifically for accumulation (27th July, 2016) and advective (13th July, 2016) days (middle and bottom, respectively).

645